Chemical Science

ROYAL SOCIETY OF CHEMISTRY

EDGE ARTICLE

View Article Online
View Journal | View Issue

Cite this: *Chem. Sci.*, 2022, **13**, 14114

All publication charges for this article have been paid for by the Royal Society of Chemistry

Chiral derivatization-enabled discrimination and on-tissue detection of proteinogenic amino acids by ion mobility mass spectrometry†

Chengyi Xie,[a] Yanyan Chen,[a] Xiaoxiao Wang,[a] Yuanyuan Song,[a] Yuting Shen,[a] Xin Diao,[a] Lin Zhu,[a] Jianing Wang *[ab] and Zongwei Cai *[a]

Received 28th June 2022
Accepted 9th November 2022

DOI: 10.1039/d2sc03604e

rsc.li/chemical-science

The importance of chiral amino acids (AAs) in living organisms has been widely recognized since the discovery of endogenous D-AAs as potential biomarkers in several metabolic disorders. Chiral analysis by ion mobility spectrometry-mass spectrometry (IMS-MS) has the advantages of high speed and sensitivity but is still in its infancy. Here, an N_α-(2,4-dinitro-5-fluorophenyl)-L-alaninamide (FDAA) derivatization is combined with trapped ion mobility spectrometry-mass spectrometry (TIMS-MS) for chiral AA analysis. For the first time, we demonstrate the simultaneous separation of 19 pairs of chiral proteinogenic AAs in a single fixed condition TIMS-MS run. The utility of this approach is presented for mouse brain extracts by direct-infusion TIMS-MS. The robust separation ability in complex biological samples was proven in matrix-assisted laser desorption/ionization (MALDI) TIMS mass spectrometry imaging (MSI) as well by directly depositing 19 pairs of chiral AAs on a tissue slide following on-tissue derivatization. In addition, endogenous chiral amino acids were also detected and distinguished. The developed methods show compelling application prospects in biomarker discovery and biological research.

Introduction

Chiral asymmetry is ubiquitous in nature. In organisms, an asymmetric feature is present, in that amino acids (AAs) are usually in the L-form, and only a few D-AAs appear. Free D-AAs and related metabolites have recently drawn increasing attention due to their important roles in physiological activities and neurological disorders.[1] It was found that D-Ser, generated from the racemization of L-serine in mammal brains,[2] is a coagonist of the *N*-methyl-D-aspartate (NMDA) receptors.[3] In addition, abnormal levels of D-Ser have been associated with neurological diseases, such as Alzheimer's disease[4] and schizophrenia.[5] D-Ser has been found in organisms other than mammals as well. It was reported that D-Ser plays a role in sleeping regulation in *Drosophila* intestine[6] and is related to epidermal vesicle release in *Ciona*.[7] However, the involvement of most D-AAs in physiological activities is still not clearly understood. Furthermore, D- and L-AAs have highly similar chemical and physical properties and differ only in their optical activity, hindering their routine separation for analysis and further biofunctional studies in complex samples. Chiral research greatly relies on the development of analytical methodologies with adequate selectivity and sensitivity to achieve the detection of low concentrations of D-AAs under the interference of abundant L-AAs in biological samples.

Electrophoretic and chromatographic techniques have been widely used for chiral analysis. In general, chiral stationary phases, chiral selectors or chiral derivatization agents (CDAs) are involved in the separation process and have been well developed in recent years,[8–12] promoting the depth and breadth of chiral research. The combination of mass spectrometry (MS) and capillary electrophoresis (CE) or liquid chromatography (LC) can further improve the performance of chiral identification because mass spectrometry can accurately determine molecular weight and provide molecular fragmentation information. Even so, their time-consuming nature limits further applications of liquid-phase separation techniques for rapid chiral assay and *in situ* imaging analysis.

Ion mobility spectrometry (IMS) largely compensates for the drawbacks of CE and LC as it provides gas-phase separation on a millisecond time scale compared to the minutes to hours for separation with CE or LC. In addition to isomeric separation[13–17] and structure elucidation,[18,19] the high speed IMS can be coupled with liquid phase separation to greatly increase the peak capacity and dynamic range by constructing a multidimensional separation system.[20,21] IMS-MS has been used for the investigation of the chiral effects of truncated amyloid-beta (Aβ) related to Alzheimer's disease.[22] Recently, it has been reported

[a]*State Key Laboratory of Environmental and Biological Analysis, Department of Chemistry, Hong Kong Baptist University, Hong Kong SAR, China. E-mail: j_wang@hkbu.edu.hk; zwcai@hkbu.edu.hk; Fax: +852-34117348; Tel: +852-34117070*

[b]*Institute for Research and Continuing Education, Hong Kong Baptist University, Hong Kong SAR, China*

† Electronic supplementary information (ESI) available. See DOI: https://doi.org/10.1039/d2sc03604e

that protonation-induced diastereomers can be separated by differential mobility spectrometry (DMS).[23] In IMS, gas-phase ions are separated according to their average collisional cross section (CCS) by the combined manipulations of the electrical field and inert-gas flow.[24] Nevertheless, enantiomers could not be separated directly by IMS since they have the same mobility in the gas phase.[25,26] Therefore, different methodologies, (i) the introduction of volatile chiral reagents into the IMS drift tube,[27] (ii) formation of noncovalent complexes,[23,25,28–33] and (iii) chemical derivatization methods,[26,34,35] have been developed for chiral IMS analysis. In general, the core principle of methods (ii) and (iii) is transforming enantiomers into diastereomers to generate CCS differences between pairs of original enantiomers in IMS. The success of the gas-phase chiral separation strategy was made possible by the development of high resolving power (*R*) IMS instrumentation, such as trapped ion mobility spectrometry (TIMS),[36] cyclic ion mobility (cIM),[37] structures for lossless ion manipulations (SLIM),[38] the U-shaped mobility analyzer (UMA),[39] DMS,[40] and so on. However, the highly similar chemical structure limits the further separation of small chiral amino acids even with high *R* IMS.[34]

With the combination of high resolving power IMS and novel chiral derivatization methods, continuous progress has been made in direct chiral IMS with increasing numbers of chiral AAs being separated using a single chiral selector.[26,34,35] In 2019, Somsen *et al.* resolved 13 proteinogenic AAs using chiral derivatization with (+)-1-(9-fluorenyl)ethyl chloroformate (FLEC).[26] Karst *et al.* developed an automated method for the separation of eight AAs by chiral derivatization with (*S*)-naproxen chloride (S-NAP) followed by TIMS-MS analysis.[34] The method was successfully used for IMS-based separation of the smallest chiral AA (*i.e.*, Ala) even in samples with high salt content. It should be noted that by optimizing the IMS conditions individually for each pair of amino acids, Guo *et al.* achieved the separation of all 19 encoded proteinogenic AAs using a steroid-based chiral derivatization reagent and a U-shaped ion mobility-mass spectrometer.[35] However, individually optimized IMS conditions may limit the application of this method for high-throughput chiral analysis and *in situ* imaging analysis. In view of the above, the development of chiral derivatization methods with fixed IMS conditions to simultaneously separate all encoded proteinogenic AAs remains an analytical challenge. The significance of achieving this goal lies in the direct detection and practical application of IMS-based chiral selectors in complex biological samples, including a large number of isomeric and isobaric interferents. Furthermore, the relative abundance of chiral AAs has been observed to vary across different areas of brain tissue,[4] providing a strong motivation to visualize chiral AA distributions by mass spectrometry imaging (MSI).

In this work, the combination of N_α-(2,4-dinitro-5-fluorophenyl)-L-alaninamide (FDAA) derivatization and TIMS-MS for chiral amino acid analysis was systematically investigated. The powerful IMS-based chiral separation ability of FDAA was demonstrated for all 19 encoded proteinogenic AAs, using the same ionic form without tedious optimization. To the best of our knowledge, FDAA derivatization achieved for the first time the successful differentiation of a mixture of 19 pairs of DL-AAs with concentration down to the nM level in a single TIMS-MS run. Moreover, the effectiveness of FDAA for AA identification was also investigated in mouse brain samples.

Experimental

Chemicals and samples

The D and L forms of arginine (Arg), alanine (Ala), tryptophan (Trp), leucine (Leu), aspartic acid (Asp), glutamine (Gln), glutamic acid (Glu), phenylalanine (Phe), and proline (Pro), as well as the D forms of asparagine (Asn), histidine (His), methionine (Met), serine (Ser), threonine (Thr), tyrosine (Tyr), and valine (Val), and the L form of isoleucine (Ile) were purchased from Aladdin Co., Ltd (Shanghai, China). L-His, D-lysine (Lys), L-Lys, L-Met, L-Thr, L-Val, L-Ser, N_α-(2,4-dinitro-5-fluorophenyl)-L-alaninamide (FDAA), N_α-(2,4-dinitro-5-fluorophenyl)-L-valinamide (FDVA), sodium bicarbonate, HPLC-grade tetrahydrofuran (THF), and 2,5-dihydroxyacetophenone (DHAP) were obtained from Sigma Aldrich Corp. (Darmstadt, Germany). D-Cysteine (Cys), L-Asn, and D-Ile were purchased from Shanghai Macklin Biochemical Co., Ltd (Shanghai, China). L-Cys was obtained from Shanghai Yuanye Biological Technology Co., Ltd (Shanghai, China). L-Tyr was purchased from Beijing Dingguo Changsheng Biotechnology Co., Ltd (Beijing, China). HPLC-grade methanol (MeOH) was obtained from VWR Chemicals (Fontenay-sous-Bois, France). AR-grade chloroform was purchased from RCI Labscan (Bangkok, Thailand). Pesticide-grade acetone was purchased from Duksan Pure Chemical Co. Ltd (Ansan, Kyonggido, South Korea). Deionized water was obtained from a Milli-Q water purification system (Millipore Corp., Bedford, MA, USA).

Sample preparation

Amino acid standard solutions were prepared separately by dissolving the solute in deionized water at the concentration of 1 mM except for Asp and Glu solutions (10 mM) which used aqueous NaOH (1 mM) as a solvent. D/L-AA mixture solutions were prepared by mixing D- and L-AAs at a 1 : 1 volume ratio. Similarly, the mixture solution of 38 AAs was prepared by mixing all AA standards at the same volume. For the determination of the enantiomeric ratio in AA mixtures, D-AAs and L-AAs with different volume ratios (0.5/99.5, 1/99, 10/90, 20/80, 30/70, 40/60, 50/50) were prepared. The preparation of mouse brain extracts and tissue slides is provided in the ESI.† For chiral derivatization, equal volumes (20 μL) of the prepared analyte solution (pure AA solution, mixed AA solution, or brain extract), aqueous sodium bicarbonate (100 mM), and the derivatization reagent (FDAA or FDVA, 5 mM) dissolved in MeOH/THF (1 : 1, v/v) were fully mixed and then incubated at 40 °C for 60 minutes. For the analysis of AA standards, all derivatized mixtures were diluted 100 times using methanol. Therefore, the final concentrations for each AA in the pure standards, racemic mixtures, and 38 AA mixtures were 3.3 μM, 1.65 μM, and 87.7 nM, respectively, except for Asp and Glu (33 μM, 165 μM, and 877 nM). For the analysis of mouse brain extracts, the

derivatized mixtures were diluted 10 fold in methanol before the direct-infusion TIMS-MS analysis.

Direct-infusion TIMS-MS

All electrospray ionization (ESI) TIMS-MS and matrix-assisted laser desorption/ionization (MALDI) TIMS-MS analyses were performed on a timsTOF fleX MALDI-2 (Bruker Daltonics, Bremen, Germany) equipped with dual ESI-MALDI sources. The ESI source was used for direct-infusion study with a flow rate of 3 μL min^{-1} and the parameters of the ion source were set as the following: end plate offset, 500 V; capillary voltage, 4000 V; nebulizer, 0.3 bar; dry gas, a flow rate of 3.5 L min^{-1} at 200 °C. For the TIMS analyzer, the accumulation time was set to 100 ms. The $1/K_0$ range (0.7–1.2 V s cm^{-2}) and ramp time (949 ms), which mainly determine the resolving power of TIMS, were kept constant throughout all direct-infusion experiments. The mass range was set to 150–1300 m/z to include all analyte ions. In addition, the tuned parameters, which also influence the detection range and sensitivity of TIMS-MS, are listed in Table S1.†

MALDI TIMS-MS

Data were acquired at 100 μm spatial resolution in M5 mode with 100% laser power at 1000 Hz and 200 shots per pixel. The ramp time and $1/K_0$ range were adjusted to 839 ms and 0.7–1.3 V s cm^{-2}. The accumulation time was 200 ms, which was determined by laser shots and frequency in the MALDI mode. Other parameters are listed in Table S2.†

Calibration

Mass and mobility calibrations were performed before the start of each experiment using the ESI-L Low Concentration Tuning Mix (Agilent Technologies, CA, USA). Since the elution voltage V_e is strongly correlated with reduced mobility of the ions,[41] the calibration curve is derived from $K_0 = a + b/V_e$, where a and b are calibration constants and were determined from known calibrant ions in the tuning mix. Before the TIMS calibration, the gas flow was fine-tuned to ensure that the V_e value of the calibrant ion at m/z 622.03 is 132 ± 1 V. The calibration process was accomplished using timsControl (Bruker Daltonics, Bremen, Germany). Then the reduced mobility of unknown analytes can be determined as long as the TIMS operating conditions remain constant.

Data analysis

The extraction of m/z, ion mobilograms, $1/K_0$, and resolving power (R) and finding of mobilogram compounds were accomplished using Compass DataAnalysis 5.3 (Bruker Daltonics, Bremen, Germany). MALDI-TIMS MS data was normalized to the root mean square value (RMS) and visualized using SCILS Lab MVS (2022b Premium 3D, Bruker Daltonics, Bremen, Germany). IMS resolution (R_{PP}) and R were calculated as $R_{PP} = 1.18(A_2 - A_1)/(\Delta A_1 + \Delta A_2)$ and $R = A/\Delta A$, respectively, where A is the $1/K_0$ value and ΔA is the full peak width at half-maximum.

Results and discussion

Single condition differentiation of nineteen chiral amino acid pairs

The differentiation of enantiomers is a prerequisite for further exploring the roles and functions of chiral amino acids in living organisms. Although continuous progress has been made in IMS-based chiral separation,[25–35] the challenge of the realization of a single IMS separation analysis for a large number of AAs in complex samples has not been overcome due to the requirement of not only high sensitivity for trace levels of chiral analytes but also the ability to distinguish enantiomers under the interference of other isobars and isomers. Given the proven potential of the chiral derivatization agent N_α-(2,4-dinitro-5-fluorophenyl)-L-alaninamide (FDAA) in chiral LC analysis,[42–45] which mainly reacts with amino group, sulfhydryl groups, and hydroxyl groups,[43] we used FDAA derivatization for IMS-based chiral separation in both standards and real samples. The derivatization reaction scheme is shown in Fig. 1A. Nucleophilic aromatic substitution of FDAA by the amino groups of amino acids leads to the transformation of enantiomers into diastereomers.[42] To clarify the chiral-IMS analysis process, the

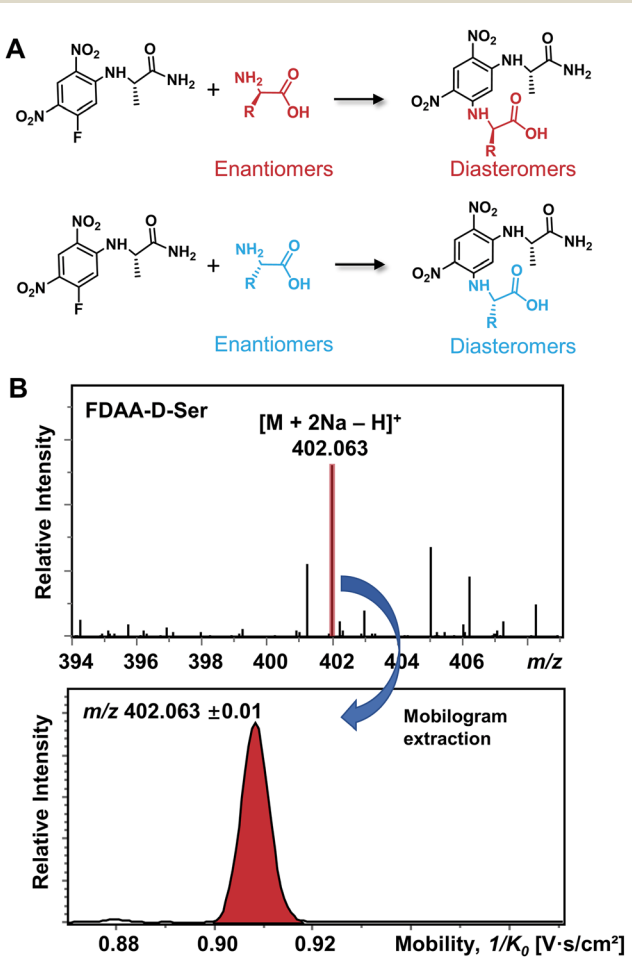

Fig. 1 (A) Chiral derivatization reaction of AAs using FDAA. (B) Mass spectrum of FDAA derivatized Ser and the corresponding extracted mobilogram at m/z 402.063 ± 0.01.

standard solution of D-Ser was selected as a representative. Fig. 1B shows the mass spectrum of the derivatized D-Ser solution after the direct-infusion analysis. Due to the use of sodium bicarbonate buffer in the reaction mixtures, $[\text{FDAA-D-Ser} + 2\text{Na} - \text{H}]^+$ is observed at m/z 402.063 in the mass spectrum. According to previous studies, the formation of metal ion adducts facilitates the differentiation of chiral amino acids,[25,26,28,29,33–35] especially the $[\text{M} + 2\text{Na} - \text{H}]^+$ ionic form of the AA derivatives.[26,35] After this reaction, a relative ion intensity (RI) of 68% ($(\text{RI} = I_{\text{product}}/(I_{\text{product}} + I_{\text{reactant}}))$[46]) was observed for FDAA-labeled Ser and an RI of 93% was observed for another derivatized AA, Trp, as shown in Fig. S1.† Since diastereomers have exactly the same molecular weight, their separation is achieved exclusively by IMS. The ion mobilogram of m/z 402.063 $\pm$ 0.01 was extracted by plotting $1/K_0$ (inverse reduced mobility; to simplify, the term "mobility" will be used) against intensity to compare the mobility distribution of the formed diastereomers (Fig. 1B lower panel).

All 19 encoded proteinogenic amino acids were investigated to evaluate the effectiveness of the FDAA derivatization and chiral separation by TIMS-MS. The extracted ion mobilograms (EIMs) of 19 pairs of FDAA-AA mixtures are presented in Fig. 2A–S. All the measurements of TIMS-MS experiments were carried out under the same instrumental settings (same TIMS and tuning parameters), enabling comparison between different pairs of diastereomers and reducing tedious optimization processes for each set of experiments. To keep the same instrumental settings, the mobility range should be set large enough to include all analytical ions while the separation performance of TIMS will be compromised. In order to quantitatively compare separation degree, the distribution of peak-to-peak resolution R_{pp} is shown in Fig. 2T. In addition to D/L mixtures, the EIMs of their pure standards (*i.e.*, D-AA and L-AA measured separately) are shown in Fig. S2.† The result confirmed that our method achieves effective separation of D/L AAs and eliminates the possibility of multiple mobility peaks caused by other factors (*i.e.* different ionization sites[47–50] or structural dynamics during transit through TIMS[51]). In general, all 19 pairs of chiral AAs could be distinguished by only selecting the ionic form of $[\text{M} + 2\text{Na} - \text{H}]^+$ without carefully optimizing the combination of reference compounds and cations. Among them, baseline or nearly baseline separation could be achieved for most chiral AAs, which is consistent with the observation that most R_{pp} values shown in Fig. 2T are over one. For the example of the smallest chiral AA, Ala, whose IMS-based separation has been reported recently,[25,33–35] baseline separation with R_{pp} of 1.36 could be achieved. All these results strongly demonstrate that FDAA is a universal CDA for the analysis of chiral AAs by TIMS. For D/L mixtures, the mobility distribution of their separated peaks in Fig. 2A–S can be aligned

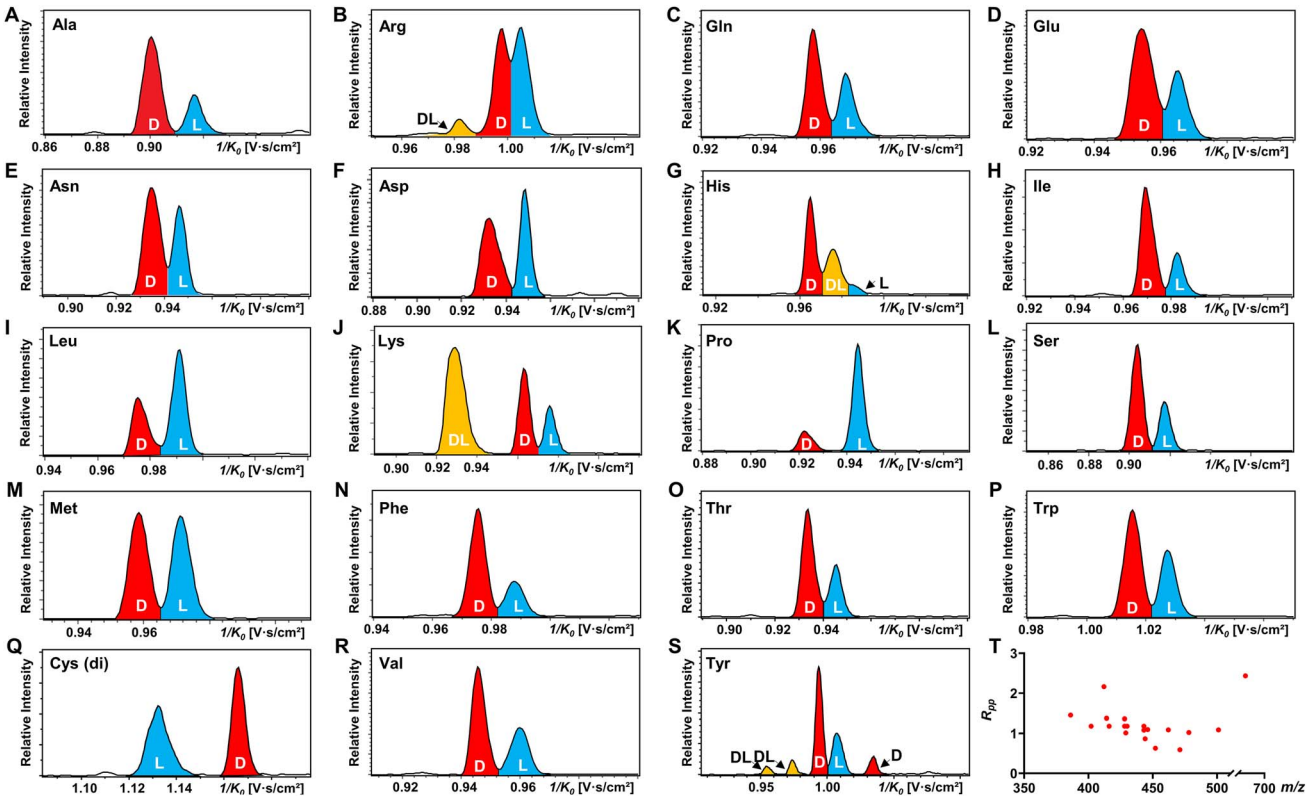

Fig. 2 TIMS differentiation of 19 chiral amino acid pairs under constant separation conditions without individual optimization for each amino acid. (A–S) EIMs of AAs (D : L = 1 : 1) after FDAA derivatization, where peaks in red, blue, and yellow traces represent D-, L-, and DL-AAs, respectively. Cys (di) indicates the bis-derivative of Cys. (T) Peak-to-peak resolution (R_{pp}) distributions of resolved chiral AAs in (A)–(S). In the case of multiple peaks, only the smallest R_{pp} value is considered.

to that of their pure enantiomeric standards measured separately and shown in Fig. S2,† indicating that FDAA-AA diastereomers are indeed separated by TIMS owing to the considerable structural difference between FDAA-AA diastereomers in the gas-phase. In comparison, representative EIMs of AAs measured before derivatization are shown in Fig. S3.† D- and L-Trp present the same mobility distribution in the ionic form of $[M + 2Na - H]^+$, and therefore only a single peak can be observed in their mixture, which means metal ion addition cannot differentiate chiral AAs directly without derivatization, as previously reported for the protonated form.[25] In addition to powerful separation ability, the use of a fixed separation condition enables the maintenance of stable separation results (*e.g.*, $1/K_0$ and R_{pp}) for various samples (*e.g.*, individuals and mixtures), facilitating the accurate and efficient identification of targeted analytes in real samples without case by case optimization.

Another chiral derivatization agent analogous to Marfey's reagent, N_α-(2,4-dinitro-5-fluorophenyl)-L-valinamide (FDVA), was introduced in this study to compare the differentiation capabilities of FDAA and FDVA for chiral amino acids. TIMS analysis for each pair of AA mixtures after FDVA derivatization was performed under the same instrumental settings as the FDAA derivatization method, and the corresponding EIMs are presented in Fig. S4.† The FDAA derivatization method showed a generally better separation ability than FDVA for chiral AAs. All AAs are resolved by FDAA derivatization, while three AAs (Ala, Arg, and Thr) could not be resolved by FDVA derivatization. The above results indicated that FDAA is a better choice for the chiral IMS analysis of amino acids.

In addition, multiple features of Arg, His, Lys, and Tyr are observed in the EIMs of AA mixtures in Fig. 2 and pure optical standards in Fig. S2† after FDAA derivatization. In the case of basic amino acids, Arg and Lys contain two primary amines, leading to different positional substitutions by FDAA. Moreover, FDAA can also react with thiols and aromatic alcohols,[43] resulting in multiple peaks in the mobility dimension for Tyr and bis-derivatives for Cys. The appearance of multiple peaks is consistent with the chromatographic separation of FDAA derivatized AAs.[43] Even though the double substitutions increase the complexity of chiral analysis, unique features for each chiral AA can be differentiated from its optical isomer by the TIMS analyzer. Aside from Cys, bis-derivatives were observed for Lys and Tyr as well (Fig. S5†). RI_{di} for bis-derivatives is only 25% for Lys and 17% for Tyr ($RI_{di} = I_{bis\text{-}product}/(I_{bis\text{-}product} + I_{mono\text{-}product} + I_{reactant})$) in comparison with mono-derivatives (65% for Lys and 56% for Tyr). Similar to Cys, baseline separation could be achieved for the bis-derivatives of

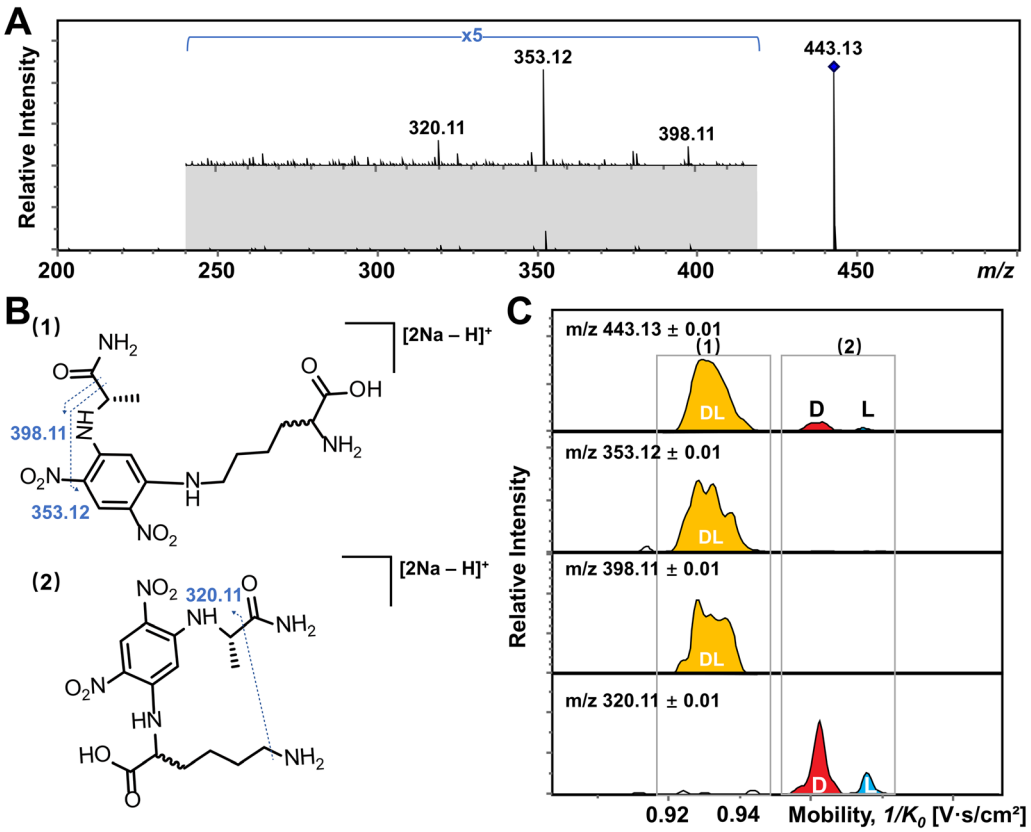

Fig. 3 Determination of the reaction site of Lys with FDAA by the combination of TIMS and tandem mass spectrometry (MS/MS). (A) MS/MS spectrum of DL-Lys after FDAA derivatization. (B) Putative fragmentation sites of Lys after the reaction of FDAA with (1) the lysyl side chain and (2) the α-amino group. (C) EIMs of product ions obtained from TIMS-MS/MS of selected ions at *m/z* 443.13. Product ions showing the same mobility distribution (*i.e.*, in the same grey frame) are derived from the same precursor ions.

DL-Lys by TIMS as shown in Fig. S6.† In contrast, DL-Tyr modified with double FDAA substitution couldn't be distinguished while better differentiation was obtained for the mono-derivatized counterpart as shown in Fig. 2S, implying that bis-derivatization does not necessarily facilitate IMS-based separation for chiral AAs. Additionally, the reaction sites can be determined by the combination of TIMS and tandem mass spectrometry (MS/MS), which is widely used for isomeric differentiation.[52,53] For the example of Lys shown in Fig. 3, product ions at *m/z* 353.12 and 398.11 are cleaved from the precursor ions with lower mobility while ions at *m/z* 320.11 are mainly produced from the higher mobility counterpart. Further structural analysis as shown in Fig. 3B can be carried out to determine the specific reaction sites corresponding to different mobility peaks of FDAA-Lys. In detail, peaks with lower mobility are derived from the reaction products of FDAA with the lysyl side chain, indicating a more compact gas-phase structure of the products when compared to the derivative produced from another positional substitution by FDAA. Baseline separation for DL-Lys was observed only for derivatization on the site of the α-amino group, which is consistent with the previous conclusion that derivatization with FDAA at the α-amino group is critical for resolution by LC-MS.[43] Similarly, the reaction sites of Tyr with FDAA can be determined as well (Fig. S7†).

The observed elution order and resolving power *R* of the resolved main peaks (Fig. 2, S6, and S8†) are listed in Table S4.† Regarding the elution order, derivatized L-AAs generally elute from the TIMS tunnel faster than their D-form counterparts, indicating a more extended gas-phase structure (higher inverse reduced mobility) of the former. The only observed exception are the bis-derivatives of D- and L-Cys, which show the opposite elution order (Fig. 2Q). The resolving power listed in Table S4† basically ranges from 100 to 200. Since the resolving power of TIMS is also related to the *m/z* of analytes,[54] in addition to the parameter settings of the TIMS analyzer, a slight shift of *R* values is observed for different AA derivatives. Considering that a resolving power of about 200 has already been achieved by other IMS instrumentations (*e.g.* UMA,[39] cIM,[37] DMS,[40] and SLIM[38]), chiral analysis of AAs by FDAA derivatization can be transferred to other IMS platforms without further improvement of sample pretreatment methods.

IMS-MS differentiation of a mixture of all encoded proteinogenic chiral amino acids in a single TIMS-MS run

To our knowledge, chiral separation of all encoded proteinogenic amino acids by a single fixed IMS-MS condition has not been achieved. Based on the results described above in this study, we further attempted to realize the possibility of distinguishing a mixture of all 19 pairs of chiral AAs in a single TIMS-MS run. The stacking EIMs of the derivatized AAs are shown in Fig. 4A arranged from front to back according to their *m/z* values observed in the mass spectrum (Fig. S9†). Separately listed mobilograms are shown in Fig. S10† to provide a clearer visualization of Fig. 4A. Leucine and isoleucine are isomers, so their mobilograms are presented together. Except for Leu and Ile, all other AAs can be differentiated by their *m/z*. Taking the example of the closest isobars of Gln and Lys among all investigated AAs, the *m/z* difference of about 0.036 was readily resolved by the quadrupole time-of-flight (qTOF) analyzer at a resolving power of 44 312 at *m/z* 443.126 (Fig. 4B). However, D/L-Leu and D/L-Ile are positional isomers that have exactly the same *m/z*. Therefore, unlike other extracted *m/z* windows where only two chiral molecules need to be separated, all four structurally similar chiral molecules need to be separated simultaneously. As presented in Fig. 4C, four peaks are recognized as D-Ile, D-Leu, L-Ile, and L-Leu according to the mobility distributions of their pure standards in Fig. S2.† The above results

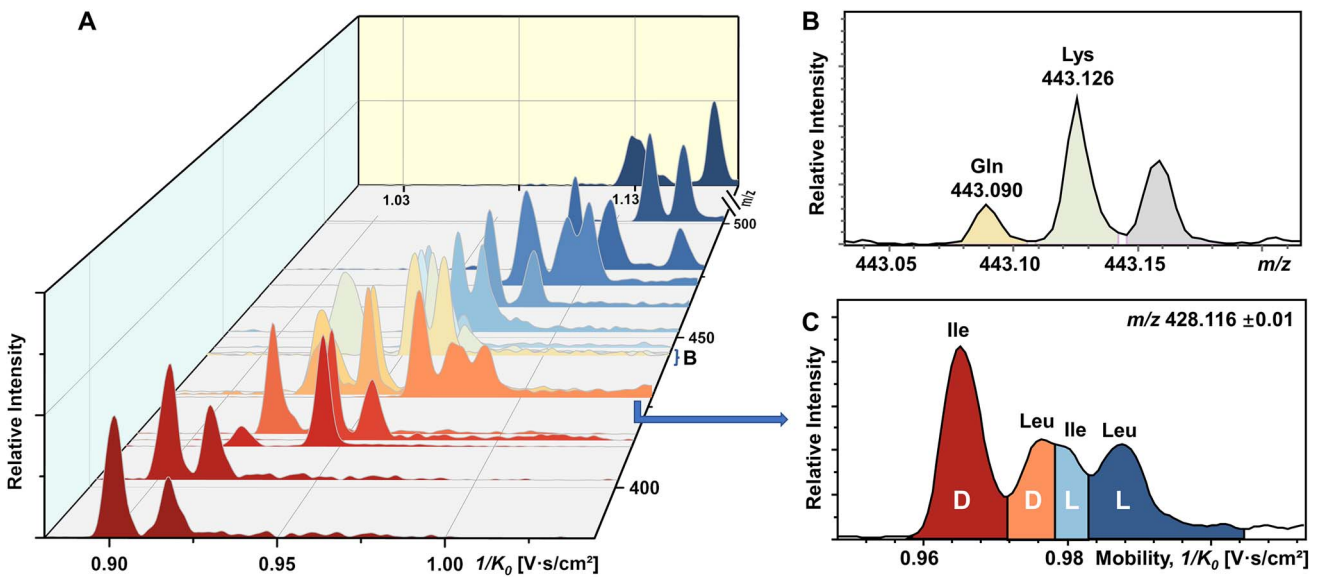

Fig. 4 Direct infusion analysis of 38 mixed amino acids by FDAA derivatization in a single TIMS-MS run. (A) Stacking EIMs of 38 chiral AAs obtained from the mixture. (B) Mass spectrum of fully resolved isobars (Gln and Lys). (C) Mobilogram extracted from *m/z* 428.116 ± 0.01 containing four resolved isomers (D-Ile, D-Leu, L-Ile, and L-Leu).

demonstrated the powerful ability of FDAA derivatization-enabled differentiation of AA isomers and enantiomers by IMS, which is important for biological samples since isomers are prevalent in metabolites and should be excluded from target analytes to protect analysis results from interference. In addition, the method is not dependent on multiple reaction monitoring (MRM) acquisition and therefore has broader instrument applicability. Furthermore, FDAA derivatization allows the separation of AAs down to 87.7 nM in the mixture, demonstrating similar sensitivity compared to previously reported derivatization methods for IMS-based chiral analysis.[26,34,35] In general, the high enantiomeric resolution, selectivity, and sensitivity of FDAA derivatization have been demonstrated, which drove us to apply this method to the analysis of real samples.

Analysis of chiral amino acids in brain extracts

Although the importance of D-amino acids in mammals has been widely recognized, such as the coagonist role of D-Ser at the NMDA receptors,[3,55] the function of most D-AAs is still not completely clear and requires more powerful separation methods for further investigation. In this study, the mouse brain was used as a biological model to explore the utility of FDAA derivatization for chiral IMS analysis. The EIMs of all observed amino acid derivatives in brain extracts are presented in Fig. S11.† In general, 15 amino acids were identified by comparing their *m*/*z* and mobility values with pure standards after FDAA derivatization. As shown in Fig. S12† as an example, FDAA derivatized Ala exhibits a peak at *m*/*z* 386.069 in the mass spectrum of mouse brain extracts. In the EIMs of *m*/*z* 386.069 ± 0.01, an interference peak (grey) is observed and excluded from the FDAA-Ala species by comparing the mobility values with the FDAA-Ala standard. Tyr and Trp are detectable but were not counted in the 15 identified amino acids due to the *m*/*z* overlap with interferent peaks. Still, the derivatized analytes can be recognized in the EIMs, as shown in Fig. S13.† However, Asp and Glu are not detected because their acidic side chains lead to poor ionization efficiency and potential ion suppression effects by complex brain extracts in positive mode ESI.

The quantitative determination of the enantiomeric ratio (er) in biological samples is of great importance since the er will change at different development stages of living organisms. The er of Ser has been demonstrated to decrease in the mouse brain with increasing age.[56] Ser and Met were chosen as examples to determine the er in the mouse brain extracts (Fig. 5). FDAA-AA standard mixtures with varying concentration ratios of D/L were used to obtain the linear calibration curves between the area ratio of D/L (*r*) and er in Fig. 5A and B. In addition, Lys containing two primary amines was analyzed as well (Fig. S14†). Good linear fit was realized for Ser, Met, and Lys with D-AA concentration down to 0.5% in the AA mixture, implying that similar ionization and derivatization efficiency are maintained with changing er even for AAs with two reaction sites, promoting the utility of FDAA derivatization for er determination in real samples. The er of Ser and Met in mouse brain extracts was determined and is shown in Fig. 5C and D. The er

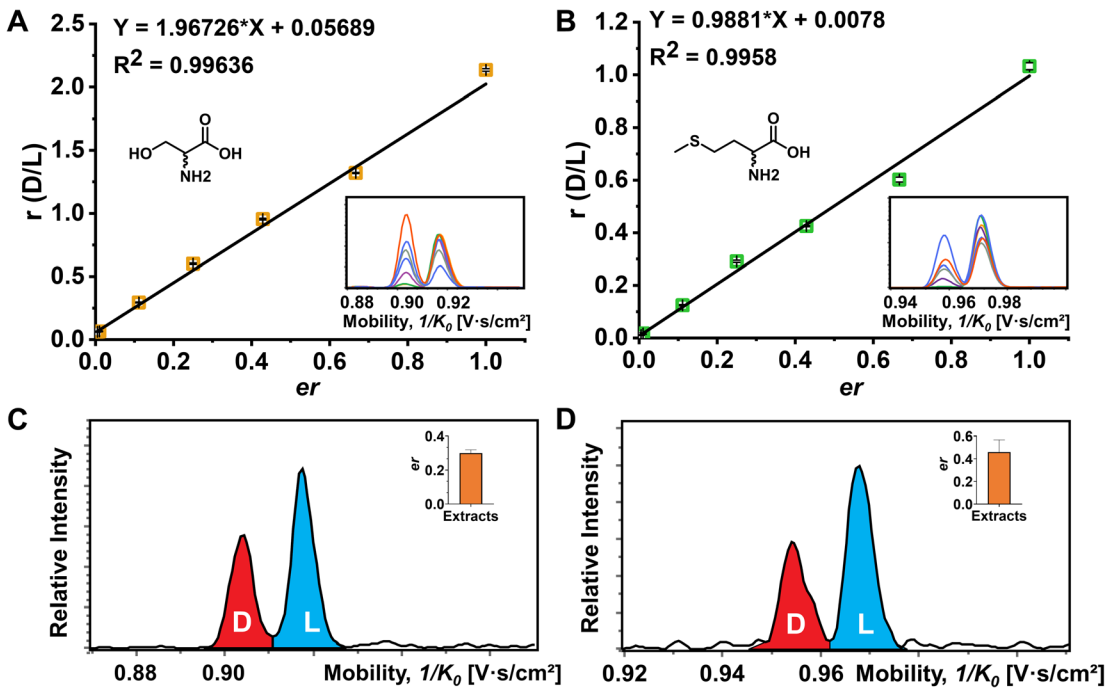

Fig. 5 Determination of the enantiomeric ratio (er) of Ser and Met. (A) The plot of peak area ratio against enantiomeric ratio (D/L) of Ser. (B) The plot of peak area ratio against enantiomeric ratio (D/L) of Met. The corresponding extracted ion mobilograms of D/L-Ser and D/L-Met at different mixing ratios are shown in the embedded images. Four technical replications of the TIMS-MS analysis were performed. (C) Extracted ion mobilograms and the corresponding er of Ser (inserted bar chart) in the mouse brain extracts. (D) Extracted ion mobilograms and the corresponding er of Met (inserted bar chart) of the mouse brain extracts. The TIMS-MS analysis for mouse brain extracts was carried out six times.

of Ser of about 30% is similar to the D-Ser% measured by LC in mouse cortex,[57] but the er of Met has not been reported yet. In summary, FDAA derivatization is demonstrated as a powerful method for chiral amino acid separation by a TIMS-MS platform.

On-tissue detection of chiral amino acids

Recently, mass spectrometry imaging has been used to reveal the spatial distribution of isomeric metabolites in biological systems.[52,58–61] Based on the FDAA-enabled chiral separation ability exhibited in tissue extracts, we further investigate the separation ability of FDAA derivatization in tissue sections by MALDI TIMS MSI. 38 AAs were directly deposited on the right half of the mouse brain section, and MSI was performed on the rectangular area covering the whole mouse brain section. In the mass spectrum shown in Fig. 6A, all *m*/*z* values of $[FDAA\text{-}AA + 2Na - H]^+$ ions are detected, demonstrating the success of the on-tissue FDAA reaction, but *m*/*z* 418.040 for Cys was excluded upon comparing its EIMs with the Cys standards shown in Fig. S15,† possibly due to the easily oxidizable properties of Cys. To increase the confidence of assignment, on-tissue MS/MS was performed for the observed derivatives. Product ions after fragmentation are shown in Table S5† and can be assigned to the corresponding fragmentation sites of ions $[FDAA\text{-}AA + 2Na - H]^+$ (Fig. S16A†). In addition, the on-tissue FDAA derivatization gave products with a high RI of 91% for Trp and 92% for Ser (Fig. S17†). Each pair of observed AAs were separated by MALDI TIMS-MS and the two-dimensional features (*m*/*z* *vs.* mobility) of the 18 pairs of AAs with defined windows were extracted and are plotted in Fig. S18,† demonstrating the separation capacity of TIMS-MS for chiral AAs after FDAA derivatization even in long-term MALDI MSI acquisition. The ion images of all separated chiral AAs are shown in Fig. 6B. For most AAs, higher ion signals can be observed in outside areas compared to the brain part, possibly due to the presence of competing molecules in the tissue region. L-Gln, D/L-Asp and D/L-Glu show the opposite trend since these amino acids have a higher abundance than other AAs in the brain tissue[57] and present relatively clear ion images in the undeposited left half of the brain section. According to

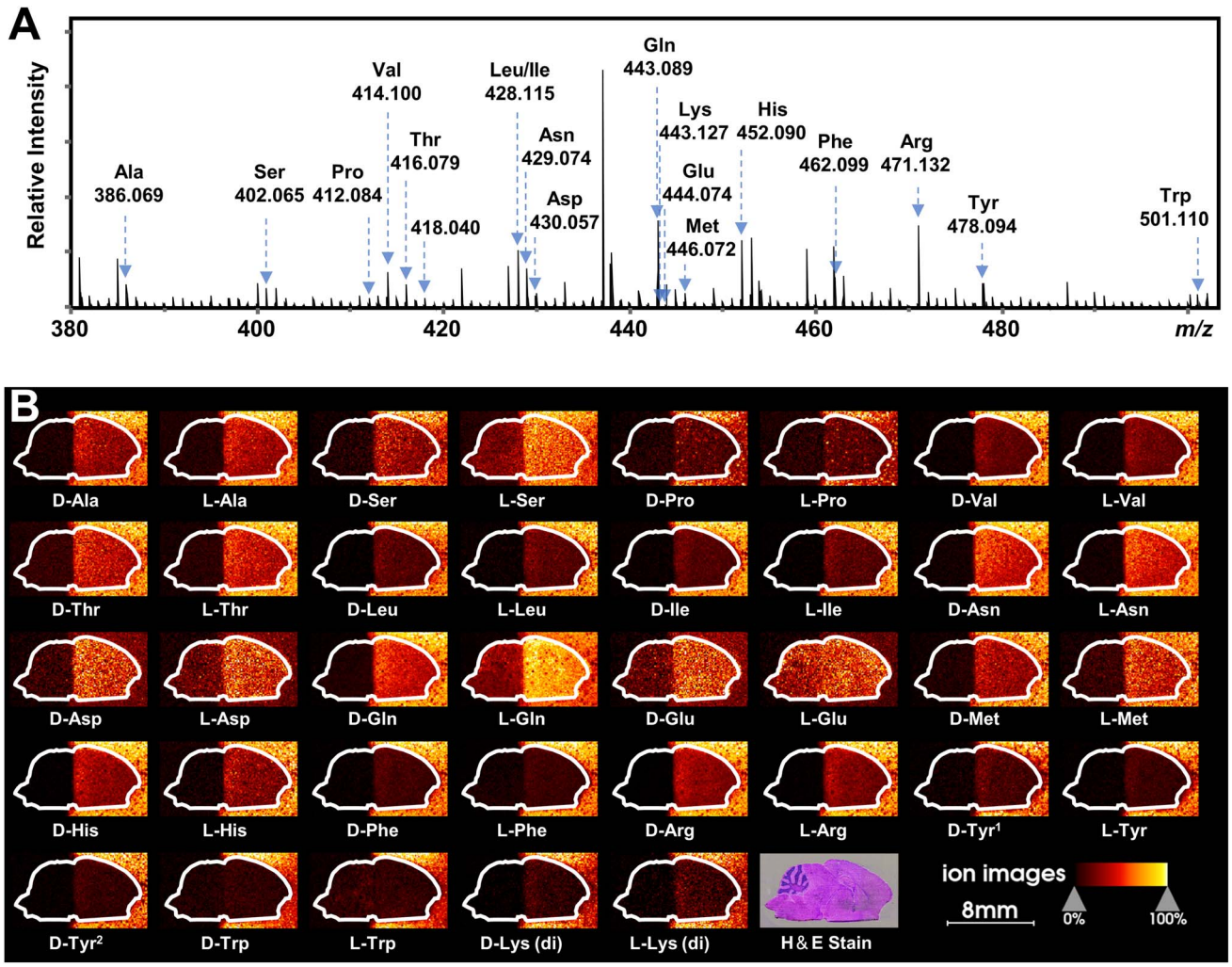

Fig. 6 MALDI TIMS MSI of chiral amino acids in mouse brain tissue after the deposition of 38 AA standards by on-tissue FDAA derivatization. (A) MALDI mass spectrum recorded from the section of mouse brain. Amino acid derivatives are assigned to AAs based on accurate mass and mobility alignments. (B) Ion images of detected chiral AAs. The extraction windows of *m*/*z* and mobility were set according to Fig. S18.†

the results of standard blending, endogenous chiral amino acids can be identified and visualized as shown in Fig. S19.† The D- and L-forms of Glu and Asp, which were not detected by direct-infusion ESI analysis, are observed by MALDI MSI, presumably caused by different ionization selectivity and polarity coverage between ESI and MALDI. Overall, these results validate the applicability of the developed method to differentiate and detect chiral amino acids in biological samples using MALDI TIMS MSI.

Conclusions

In this study, a powerful TIMS-based method was developed for chiral amino acid analysis using FDAA derivatization. Chiral separation was achieved for all 19 pairs of encoded proteinogenic amino acids labeled with FDAA using the same ionic form, avoiding the optimization of reference compounds and metal ions for specific analytes. Although derivatized Lys and Tyr presented multiple IMS peaks due to their various reaction sites with FDAA, the exact substitution site can be determined by TIMS-MS/MS. The high selectivity and sensitivity of FDAA combined with TIMS-MS for chiral discrimination were also demonstrated in the simultaneous separation of a mixture of 38 AAs (19 pairs of DL-forms) down to the nM concentration range. Using the FDAA derivatization method, we detected 15 AAs simultaneously and excluded isomeric and isobaric interference in mouse brain extracts. As a proof of concept, the er was determined for Ser and Met in the brain extracts. The separation capacity of FDAA derivatization was also proved in MALDI TIMS MSI of a mouse brain section with the deposition of 38 AAs. In general, the developed method shows powerful potential for IMS-based separation of chiral amino acids both in ESI analysis and MALDI MSI, which widens the path to the further investigation of biological functions and mechanisms of chiral molecules in complex biological samples. In addition, the effectiveness of this CDA for other metabolites and peptides is also well worth studying to expand potential IMS-based applications.

Data availability

The supporting data for the findings of this study are available within the article and ESI.†

Author contributions

J. Wang and Z. Cai conceived and supervised the project, and revised the manuscript. J. Wang, Z. Cai, and C. Xie designed the experiments. Y. Song, Y. Shen, and C. Xie prepared samples. Y. Chen and X. Wang performed animal experiments. C. Xie collected IMS-MS data and prepared the first draft of the manuscript. Y. Chen., X. Diao, L. Zhu, and C. Xie participated in data analysis. All authors were involved in the preparation of the manuscript.

Conflicts of interest

There are no conflicts to declare.

Acknowledgements

The authors would like to acknowledge Dr Xiaobo Xie at the Analytical & Testing Center, Sichuan University, for helpful discussion on chemical derivatization. This work was supported by The Shenzhen Science and Technology Innovation Commission (2021Szvup134), a SKLEBA Research Grant (SKLP_2021_P04), and a Start-up Grant from Hong Kong Baptist University. Experimental protocols were approved by the Hong Kong Baptist University Committee on the Use of Human and Animal Subjects in Teaching and Research.

References

1 H. Wolosker, R. Panizzutti and J. D. Miranda, *Neurochem. Int.*, 2002, **41**, 327–332.
2 H. Wolosker, K. N. Sheth, M. Takahashi, J.-P. Mothet, R. O. Brady, C. D. Ferris and S. H. Snyder, *Proc. Natl. Acad. Sci. U. S. A.*, 1999, **96**, 721–725.
3 J.-P. Mothet, A. T. Parent, H. Wolosker, R. O. Brady, D. J. Linden, C. D. Ferris, M. A. Rogawski and S. H. Snyder, *Proc. Natl. Acad. Sci. U. S. A.*, 2000, **97**, 4926–4931.
4 C. Madeira, M. V. Lourenco, C. Vargas-Lopes, C. K. Suemoto, C. O. Brandão, T. Reis, R. E. P. Leite, J. Laks, W. Jacob-Filho, C. A. Pasqualucci, L. T. Grinberg, S. T. Ferreira and R. Panizzutti, *Transl. Psychiatry*, 2015, **5**, e561.
5 M. A. Calcia, C. Madeira, F. V. Alheira, T. C. S. Silva, F. M. Tannos, C. Vargas-Lopes, N. Goldenstein, M. A. Brasil, S. T. Ferreira and R. Panizzutti, *Schizophr. Res.*, 2012, **142**, 83–87.
6 X. Dai, E. Zhou, W. Yang, X. Zhang, W. Zhang and Y. Rao, *Nat. Commun.*, 2019, **10**, 1986.
7 G. Krasovec, A. Hozumi, T. Yoshida, T. Obita, M. Hamada, A. Shiraishi, H. Satake, T. Horie, H. Mori and Y. Sasakura, *Sci. Adv.*, 2022, **8**, eabn3264.
8 S. Bernardo-Bermejo, E. Sánchez-López, M. Castro-Puyana and M. L. Marina, *TrAC, Trends Anal. Chem.*, 2020, **124**, 115807.
9 I. Ilisz, A. Péter and W. Lindner, *TrAC, Trends Anal. Chem.*, 2016, **81**, 11–22.
10 G. Sicoli, Z. Jiang, L. Jicsinsky and V. Schurig, *Angew. Chem., Int. Ed.*, 2005, **44**, 4092–4095.
11 T. Tanaka, T. Sugita, S. Tokuji, S. Saito and A. Osuka, *Angew. Chem., Int. Ed.*, 2010, **49**, 6619–6621.
12 T. Miyabe, H. Iida, A. Ohnishi and E. Yashima, *Chem. Sci.*, 2012, **3**, 863–867.
13 Q. Wu, J.-Y. Wang, D.-Q. Han and Z.-P. Yao, *TrAC, Trends Anal. Chem.*, 2020, **124**, 115801.
14 Z. Chen, M. S. Glover and L. Li, *Curr. Opin. Chem. Biol.*, 2018, **42**, 1–8.
15 E. Mucha, A. Stuckmann, M. Marianski, W. B. Struwe, G. Meijer and K. Pagel, *Chem. Sci.*, 2019, **10**, 1272–1284.
16 X. Zheng, N. A. Aly, Y. Zhou, K. T. Dupuis, A. Bilbao, V. L. Paurus, D. J. Orton, R. Wilson, S. H. Payne, R. D. Smith and E. S. Baker, *Chem. Sci.*, 2017, **8**, 7724–7736.
17 N. Sahota, D. I. AbuSalim, M. L. Wang, C. J. Brown, Z. Zhang, T. J. El-Baba, S. P. Cook and D. E. Clemmer, *Chem. Sci.*, 2019, **10**, 4822–4827.

18 L. M. Young, L.-H. Tu, D. P. Raleigh, A. E. Ashcroft and S. E. Radford, *Chem. Sci.*, 2017, **8**, 5030–5040.
19 J. A. Picache, B. S. Rose, A. Balinski, K. L. Leaptrot, S. D. Sherrod, J. C. May and J. A. McLean, *Chem. Sci.*, 2019, **10**, 983–993.
20 Y. Cong, K. Motamedchaboki, S. A. Misal, Y. Liang, A. J. Guise, T. Truong, R. Huguet, E. D. Plowey, Y. Zhu, D. Lopez-Ferrer and R. T. Kelly, *Chem. Sci.*, 2021, **12**, 1001–1006.
21 E. S. Baker, E. A. Livesay, D. J. Orton, R. J. Moore, W. F. Danielson, D. C. Prior, Y. M. Ibrahim, B. L. LaMarche, A. M. Mayampurath, A. A. Schepmoes, D. F. Hopkins, K. Tang, R. D. Smith and M. E. Belov, *J. Proteome Res.*, 2010, **9**, 997–1006.
22 G. Li, K. DeLaney and L. Li, *Nat. Commun.*, 2019, **10**, 5038.
23 C. Ieritano, J. C. Yves Le Blanc, B. B. Schneider, J. R. Bissonnette, A. Haack and W. S. Hopkins, *Angew. Chem., Int. Ed.*, 2022, **61**, e202116794.
24 J. C. May and J. A. McLean, *Anal. Chem.*, 2015, **87**, 1422–1436.
25 C. Xie, L. Gu, Q. Wu, L. Li, C. Wang, J. Yu and K. Tang, *Anal. Chem.*, 2021, **93**, 859–867.
26 R. Pérez-Míguez, B. Bruyneel, M. Castro-Puyana, M. L. Marina, G. W. Somsen and E. Domínguez-Vega, *Anal. Chem.*, 2019, **91**, 3277–3285.
27 P. Dwivedi, C. Wu, L. M. Matz, B. H. Clowers, W. F. Siems and H. H. Hill, *Anal. Chem.*, 2006, **78**, 8200–8206.
28 V. Domalain, M. Hubert-Roux, V. Tognetti, L. Joubert, C. M. Lange, J. Rouden and C. Afonso, *Chem. Sci.*, 2014, **5**, 3234–3239.
29 X. Yu and Z.-P. Yao, *Anal. Chim. Acta*, 2017, **981**, 62–70.
30 J. D. Zhang, K. M. M. Kabir and W. A. Donald, *Anal. Chim. Acta*, 2018, **1036**, 172–178.
31 J. D. Zhang, K. M. Mohibul Kabir, H. E. Lee and W. A. Donald, *Int. J. Mass Spectrom.*, 2018, **428**, 1–7.
32 G. Nagy, C. D. Chouinard, I. K. Attah, I. K. Webb, S. V. B. Garimella, Y. M. Ibrahim, E. S. Baker and R. D. Smith, *Electrophoresis*, 2018, **39**, 3148–3155.
33 S. Yang, L. Gu, F. Wu, X. Dai, F. Xu, Q. Li, X. Fang, S. Yu and C.-F. Ding, *Talanta*, 2022, **243**, 123363.
34 J. M. Will, A. Behrens, M. Macke, C. D. Quarles and U. Karst, *Anal. Chem.*, 2021, **93**, 878–885.
35 Y. Li, B. Zhou, K. Wang, J. Zhang, W. Sun, L. Zhang and Y. Guo, *Anal. Chem.*, 2021, **93**, 13589–13596.
36 F. Fernandez-Lima, D. A. Kaplan, J. Suetering and M. A. Park, *Int. J. Ion Mobility Spectrom.*, 2011, **14**, 93–98.
37 K. Giles, J. Ujma, J. Wildgoose, S. Pringle, K. Richardson, D. Langridge and M. Green, *Anal. Chem.*, 2019, **91**, 8564–8573.
38 L. Deng, I. K. Webb, S. V. B. Garimella, A. M. Hamid, X. Zheng, R. V. Norheim, S. A. Prost, G. A. Anderson, J. A. Sandoval, E. S. Baker, Y. M. Ibrahim and R. D. Smith, *Anal. Chem.*, 2017, **89**, 4628–4634.
39 K. Wang, R. Qiu, X. Zhang, K. J. Gillig and W. Sun, *Anal. Chem.*, 2020, **92**, 8356–8363.
40 A. A. Shvartsburg, T. A. Seim, W. F. Danielson, R. Norheim, R. J. Moore, G. A. Anderson and R. D. Smith, *J. Am. Soc. Mass Spectrom.*, 2013, **24**, 109–114.
41 M. Chai, M. N. Young, F. C. Liu and C. Bleiholder, *Anal. Chem.*, 2018, **90**, 9040–9047.
42 R. Bhushan and H. Brückner, *Amino Acids*, 2004, **27**, 231–247.
43 K. Fujii, Y. Ikai, T. Mayumi, H. Oka, M. Suzuki and K. Harada, *Anal. Chem.*, 1997, **69**, 3346–3352.
44 P. Marfey, *Carlsberg Res. Commun.*, 1984, **49**, 591–596.
45 S. Sethi, J. Martens and R. Bhushan, *Biomed. Chromatogr.*, 2021, **35**, e4990.
46 G. Feng, M. Gao, L. Wang, J. Chen, M. Hou, Q. Wan, Y. Lin, G. Xu, X. Qi and S. Chen, *Nat. Commun.*, 2022, **13**, 2652.
47 G. Nagy, I. K. Attah, S. V. B. Garimella, K. Tang, Y. M. Ibrahim, E. S. Baker and R. D. Smith, *Chem. Commun.*, 2018, **54**, 11701–11704.
48 C. Xie, L. Li, Q. Wu, P. Guan, C. Wang, J. Yu and K. Tang, *Talanta*, 2021, **225**, 121903.
49 P. Guan, C. Xie, L. Li, X. Fang, F. Wu, J. J. Hu and K. Tang, *Talanta*, 2021, **230**, 122348.
50 C. Xie, Q. Wu, S. Zhang, C. Wang, W. Gao, J. Yu and K. Tang, *Talanta*, 2020, **211**, 120719.
51 D. Morsa, E. Hanozin, G. Eppe, L. Quinton, V. Gabelica and E. D. Pauw, *Anal. Chem.*, 2020, **92**, 4573–4582.
52 H. Zhang, M. Xu, X. Shi, Y. Liu, Z. Li, J. C. Jagodinsky, M. Ma, N. V. Welham, Z. S. Morris and L. Li, *Chem. Sci.*, 2021, **12**, 8115–8122.
53 G. Feng, Y. Hao, L. Wu and S. Chen, *Chem. Sci.*, 2020, **11**, 7244–7251.
54 D. R. Hernandez, J. D. DeBord, M. E. Ridgeway, D. A. Kaplan, M. A. Park and F. Fernandez-Lima, *Analyst*, 2014, **139**, 1913–1921.
55 M. J. Schell, M. E. Molliver and S. H. Snyder, *Proc. Natl. Acad. Sci. U. S. A.*, 1995, **92**, 3948–3952.
56 J.-M. Billard, *J. Pharm. Biomed. Anal.*, 2015, **116**, 18–24.
57 C. A. Weatherly, S. Du, C. Parpia, P. T. Santos, A. L. Hartman and D. W. Armstrong, *ACS Chem. Neurosci.*, 2017, **8**, 1251–1261.
58 D. Unsihuay, P. Su, H. Hu, J. Qiu, S. Kuang, Y. Li, X. Sun, S. K. Dey and J. Laskin, *Angew. Chem., Int. Ed.*, 2021, **60**, 7559–7563.
59 A. Bednařík, S. Bölsker, J. Soltwisch and K. Dreisewerd, *Angew. Chem., Int. Ed.*, 2018, **57**, 12092–12096.
60 F. Wäldchen, B. Spengler and S. Heiles, *J. Am. Chem. Soc.*, 2019, **141**, 11816–11820.
61 M. R. L. Paine, B. L. J. Poad, G. B. Eijkel, D. L. Marshall, S. J. Blanksby, R. M. A. Heeren and S. R. Ellis, *Angew. Chem., Int. Ed.*, 2018, **57**, 10530–10534.